

Efficiency and Physical Limitations of Adiabatic Direct Energy Conversion in Axisymmetric Fields

J.-M. Rax*

*Andlinger Center for Energy and Environment, Princeton University,
Princeton University, Princeton NJ 08544, USA and
IJCLab, Université de Paris-Saclay, 91405 Orsay, France*

E. J. Kolmes and N. J. Fisch

*Department of Astrophysical Sciences, Princeton University, Princeton NJ 08544, USA
(Dated: October 22, 2024)*

We describe and analyze a new class of direct energy conversion schemes based on the adiabatic magnetic drift of charged particles in axisymmetric magnetic fields. The efficiency of conversion as well as the geometrical and dynamical limitations of the recoverable power are calculated. The geometries of these axisymmetric field configurations are suited for direct energy conversion in radiating advanced aneutronic reactors and in advanced divertors of deuterium-tritium tokamak reactors. The E cross B configurations considered here do not suffer from the classical drawbacks and limitations of thermionic and magnetohydrodynamic high temperature direct energy conversion devices.

I. INTRODUCTION

Part of the internal energy content of a thermodynamical system can be extracted to produce useful work. Under reversible extraction conditions the allowed maximum extracted work is given by the free energy difference between the initial and final states [1, 2]. The *free energy content* of a system is always lower than its total *internal energy content*. Their difference is proportional to the temperature and the entropy which are always positive. Moreover, entropy production due to irreversible operations decreases the fraction of the internal energy that can be converted into useful work.

Energy conversion underlies many of the technologies that have been proposed to decarbonize the world's energy infrastructure. In addition to economic and environmental considerations, the efficiency of free energy extraction is one of the most important factors determining the relative merits of different technologies [3].

Thermodynamical energy conversion systems are usually based on simple non equilibrium states displaying gradients of intensive variables. The most common thermodynamical non equilibrium states used as free energy sources in classical conversion devices involve (i) pressure, (ii) temperature and (iii) chemical potential gradients [4]. Pressure gradients can be relaxed in turbines to produce mechanical work with a high conversion efficiency. Steady state free energy extraction associated with a simple temperature differential is limited by the Carnot's reversible efficiency at zero power and by the Curzon-Alborn-Novikov-Chambadal endoreversible efficiency at maximum power [5–7]. Chemical potential differences can be efficiently converted in electrochemical devices but are, unfortunately, usually relaxed through

open air combustion to sustain a temperature gradient in combustion driven systems.

Besides classical thermal conversion schemes, direct energy conversion (DEC) schemes such as magnetohydrodynamic (MHD) generators, thermoionic diodes (TI), photovoltaic (PV) and redox (RX) cells of the hydrogen type have been recognized to offer the potential of significant conversion efficiency as they avoid the inefficient steps requiring the cooling/heating of a compressed/expanded gas [8–10]. The basic principles of a DC electric power DEC generator is illustrated in Fig. 1-(a). Two steps are required: (i) free charge generation at a rate dN/dt followed by (ii) charge separation with a force $\pm F$ on positive and negative particles. The resulting flow of current must be oriented such that it provides power to an electric field E sustained between two electrodes separated by a gap width h .

A device's current-voltage (I - U) characteristic describes how its efficiency changes as its power throughput increases. Under ideal operations, the current-voltage “square” characteristic of this ideal DEC generator is illustrated in Fig. 1-(b). The short circuit current I_0 is given by

$$I_0 = 2q \frac{dN}{dt} \quad (1)$$

where q is the single particle charge. The open circuit voltage

$$V_0 = \frac{Fh}{q} \quad (2)$$

is reached when the electric force $\pm qE = \pm qU/h$ balances the separating force $\pm F$.

When non ideal processes are taken into account the “square” ideal characteristic becomes either a curve of the concave (TI) or convex (PV and RX) type, or simply a resistive straight line (MHD), depicted by the three

* Electronic mail: jean-marcel.rax@universite-paris-saclay.fr

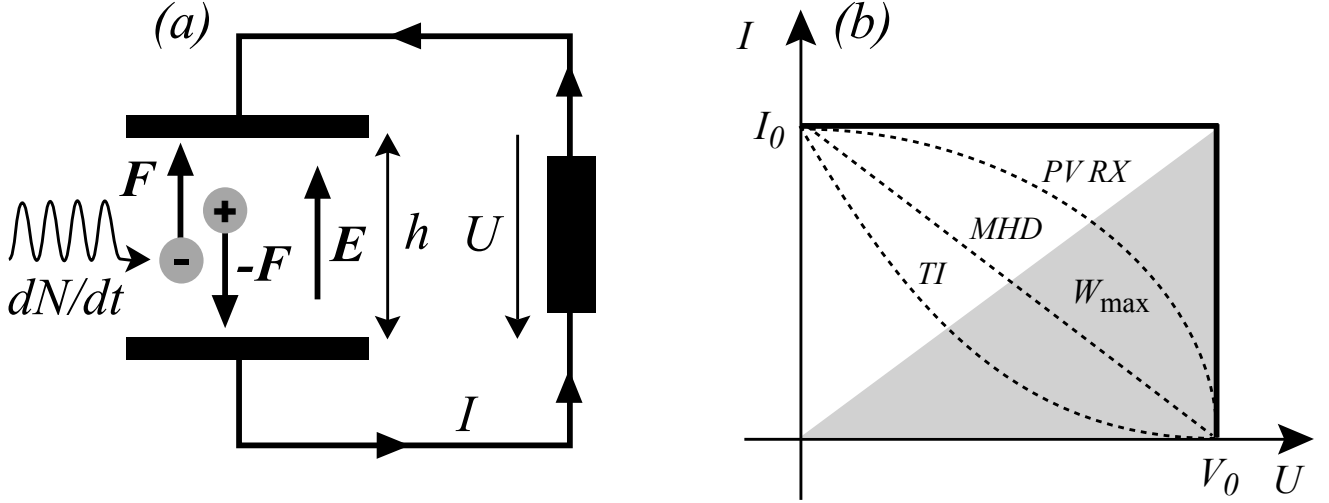


FIG. 1. (a) Basic layout of a DC electric power DEC generator, (b) ideal and non-ideal current-voltage characteristics (corresponding to the solid and dashed curves, respectively).

dotted curves in Fig. 1-(b) [8]. The maximum power W_{\max} that can be delivered to the external load from an ideal generator is

$$W_{\max} = I_0 U_0 / 2 = Fh (dN/dt). \quad (3)$$

The force F used in DEC devices is typically of a statistical nature: thermodynamical forces associated with the gradient of an intensive variable such as pressure, temperature or chemical potential. In the new class of plasma DEC presented and analyzed here the force F is the centrifugal force due to the curvature of the magnetic field lines and the diamagnetic force due to the gradient of the magnetic field strength. These are in fact thermal forces because their effects are proportional to the kinetic/thermal energy of the particles. This kinetic/thermal energy can be transformed into DC electric power through the design of a dedicated field configuration.

In TI diodes F is associated with the pressure/temperature gradient of the free electrons emitted by the hot cathode. Ions remain bounded in the cathode lattice and sustain a phonon gas rather than flowing. In MHD generators F is the friction force of the flowing neutral part of the weakly ionized plasma. In PV generators F is a chemical potential gradient resulting from the chemical potential difference between the two sides of the PV junction.

The type of DEC generator illustrated in Fig. 1-(a) is well suited when the separating force F acts in opposite directions on electrons and ions. If the force F is insensitive to the sign of the charges we can either: (i) immobilize one type of particle or (ii) use an E cross B configuration where the $\mathbf{F} \times \mathbf{B}/qB^2$ drift velocity separates the charges. An ideal E cross B configuration is

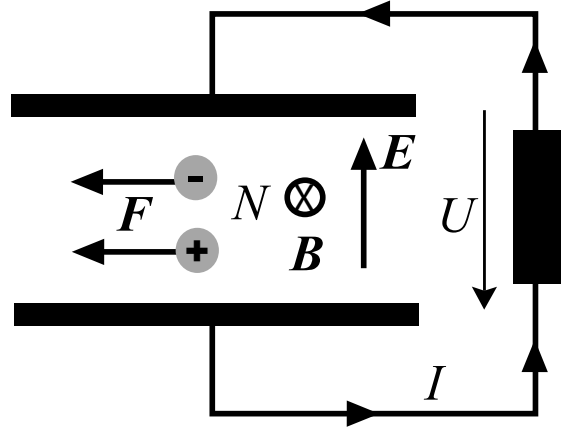


FIG. 2. An illustration of an $\mathbf{E} \times \mathbf{B}$ -type configuration. A force \mathbf{F} acts similarly on both positive and negative charged particles, so the resulting $\mathbf{F} \times \mathbf{B}$ drifts separate the charges.

illustrated in Fig. 2. For a small voltage drop U and a steady state population of $2N$ charged particles in the electrode gap, the ideal power W_0 of the generator is the product of the drift velocity F/qB times the electric force qE :

$$W_0 = 2NFE/B. \quad (4)$$

The past decades witnessed the massive development of PV and RX cell DEC generators which are now produced on a fully developed industrial scale. High temper-

ature TI and MHD DEC generators performances remain below the requirement to envision an industrial scale development. Despite the lack of industrial scale achievements, the continuous interest for TI and MHD stems from the fact that they operate at high temperatures: (i) for a given amount of energy, high temperature heat offers the potential of a far better conversion than low temperature heat, (ii) for the same power high temperature MHD and TI systems occupy a smaller footprint than classical systems.

Very high temperature heat is produced in thermonuclear reactors, (i) in the form of a high temperature plasma flow at the level of the divertor in $^2\text{D}/^3\text{T}$ tokamak reactors, or (ii) in the form of high intensity short wavelength radiation in advanced neutronless $^1\text{P}/^{11}\text{B}$ reactors. An efficient high temperature DEC scheme would be very beneficial for $^2\text{D}/^3\text{T}$ and $^1\text{P}/^{11}\text{B}$ fusion schemes. Several processes have been put forward to achieve direct conversion of thermonuclear energy [11], such as cusp configurations [12], traveling waves [13] and advanced electrostatic configurations [14, 15] or electrostatic and magnetostatic configurations of the E cross B type [16]. In this work we analyze a class of high temperature E cross B type DEC scheme free from the usual drawbacks of MHD and TI devices. The drawbacks of TI and MHD high temperature DEC devices have been known for a long time. To mention a few: the occurrence of space charge limited flow in vacuum TI diodes and the erosion of the edge electrodes in MHD generators put severe restrictions on the efficiency of such generators.

For example, let us consider a thermionic diode illustrated in Fig. 3-(a). A high-temperature source sustains a temperature difference between a hot cathode (T_c) and a cold anode ($T_a \ll T_c$). Thermionic emission, described by Richardson-Dushman's law [17], takes place at the inner surface of the cathode and electrons, with mass m , work against an electric field E during their transit from the cathode toward the anode.

Under optimal conditions the voltage U of such an electric generator is given by the relation $mv^2 = 2qU$ where $v \sim \sqrt{k_B T_c/m}$ is the average emission velocity. However, the heat driven current I is limited by Child-Langmuir's law, limiting the current density to a value J_{CL} [A/m^2] given by

$$J_{CL} = 2\varepsilon_0 m v^3 / 9 q h^2, \quad (5)$$

where h is the anode-cathode gap width. Thus, to extract significant power, an impractically tiny gap is needed. Moreover, beside the electron flux described by J_{CL} , the black-body flux of photons J_{BB} [W/m^2] provides a thermal short circuit dramatically lowering the conversion efficiency when h is small,

$$J_{BB} = \pi^2 k_B^4 T_c^4 / 15 \hbar^3 c^2, \quad (6)$$

where \hbar is Planck's constant. To avoid these drawbacks an E cross B configuration, illustrated in Fig. 3-(b), has

been proposed [18]. The current across the magnetic B field is no longer limited to J_{CL} and J_{BB} no longer heats up the cold anode, but the ballistic coupling between the cathode and the anode turn out to be inefficient because of the dispersion in the velocities of the electrons. Other mitigations of the TI drawbacks, such as the use of plasma TI diode rather than vacuum TI diodes [19], have been considered but none of them have made it possible to achieve the expected high conversion efficiency.

Nevertheless, E cross B configurations have proven their usefulness in MHD generator designs used to convert the free enthalpy of a hot weakly ionized plasma flow into DC electric power. This E cross B configuration is illustrated in Fig. 4-(a). A weakly ionized plasma flows, with a velocity \mathbf{v} along x , across a magnetic field \mathbf{B} directed along the z axis [20]. Electrons and ions set up a current \mathbf{j} under the influence of the $\mathbf{v} \times \mathbf{B}$ force. This current provides power to the electric field \mathbf{E} along the y axis. Energy conservation is ensured as the $\mathbf{j} \times \mathbf{B}$ force slows down the flow along the x axis. The short circuiting of the y currents provides another E cross B configuration beside the segmented Faraday configuration illustrated in Fig. 4-(a): the Hall configuration illustrated in Fig. 4-(b). The basic physical principles and main limitations of Faraday and Hall MHD DEC generators can be found in classical textbooks Ref. [21, 22]. Despite the simplicity and effectiveness of the physical principles put at work in Faraday and Hall generators, the management of a hot weakly ionized collisional plasma flow has proven to be difficult and MHD generators did not find their way to industrial development up to now.

The use of $\mathbf{E} \times \mathbf{B}$ configurations aimed at DEC is not restricted to advanced TI and classical MHD generators illustrated in Figures 3 and 4. We will describe and analyze in this paper another $\mathbf{E} \times \mathbf{B}$ configuration where the thermal energy of charged particles is converted to a DC electromotive force in very particular types of inhomogeneous magnetic and electric fields.

This new configuration does not suffer from the major drawbacks of the TI scheme and the MHD scheme. The Child-Langmuir law limitation does not apply and electrode erosion is minimized as the charged particles strike the electrodes at low energy. This configuration also has its own advantages: (i) the energy extraction rate is exponential with respect to time and (ii) the closed field line topology minimizes plasma losses. Besides the topology, the geometry is particularly pertinent for high temperature conversion in fusion reactors. The proposed configuration can be understood as a way of converting plasma kinetic energy into electricity. It can also be understood as a technique for capturing radiation, if that radiation is used to ionize neutrals and the energy is captured from the resulting charged particles.

This paper is organized as follows. In the next section we describe the way to arrange coils and electrode plates in poloidal and toroidal axisymmetric configurations in order to extract the thermal energy of a plasma. We analyze the energy exchange between charged particles and

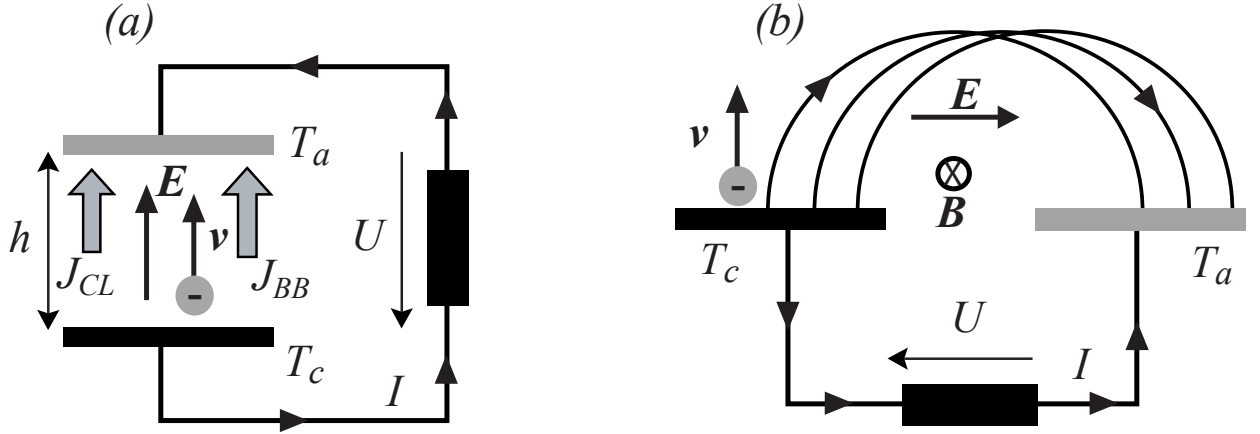


FIG. 3. Two thermionic diode configurations: (a) the basic configuration, in which thermionic emission ejects electrons parallel to an electric field, and (b) a modified configuration, in which a magnetic field is used to avoid the Child-Langmuir and blackbody limitations on the attainable current.

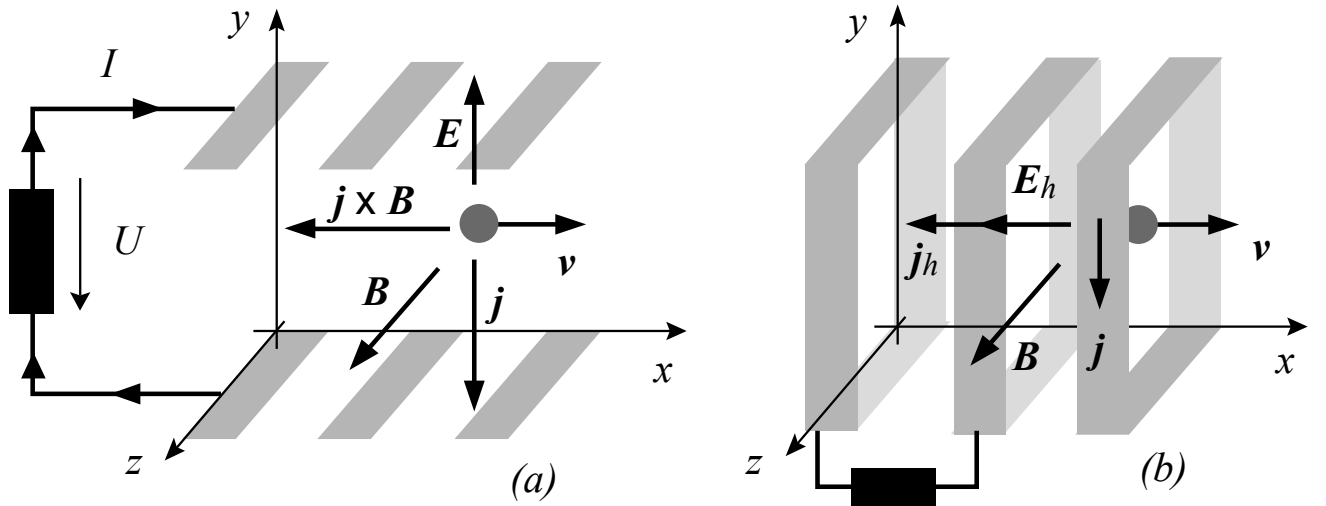


FIG. 4. Two MHD generator configurations: (a) the Faraday configuration and (b) the Hall configuration.

the electric field which provide the electromotive force of the generator in these new $\mathbf{E} \times \mathbf{B}$ configurations in Sections III and IV. We calculate the efficiency and the irreducible physical limitations on the power delivered by toroidal DEC generator in Sections V and VI. We do not consider the limitations associated with the stress on the material in a high temperature environment. This paper is instead devoted to an analysis of the physical principles. The adaptation of these DEC scheme to $^2\text{D}/^3\text{T}$ tokamak reactors and $^1\text{P}/^{11}\text{B}$ advanced reactors is briefly considered in Section VII. The last section summarizes our new results and gives our conclusions.

II. $\mathbf{E} \times \mathbf{B}$ COOLING IN POLOIDAL AND TOROIDAL CONFIGURATIONS

The design of a hot plasma DEC device requires the identification of a structure such that the motion of the charged particles is slowed down by an electric field sustained between two electrodes. As a result of global energy conservation this $\mathbf{E} \times \mathbf{B}$ electric cooling of a hot plasma results in the sustainment of an electromotive force when the electrode circuit is closed on an external load.

The magnetic drift velocity is proportional to $\mathbf{B} \times \nabla B$ and to the thermal energy content of the plasma particles. The sign of the resulting power transfer between the hot

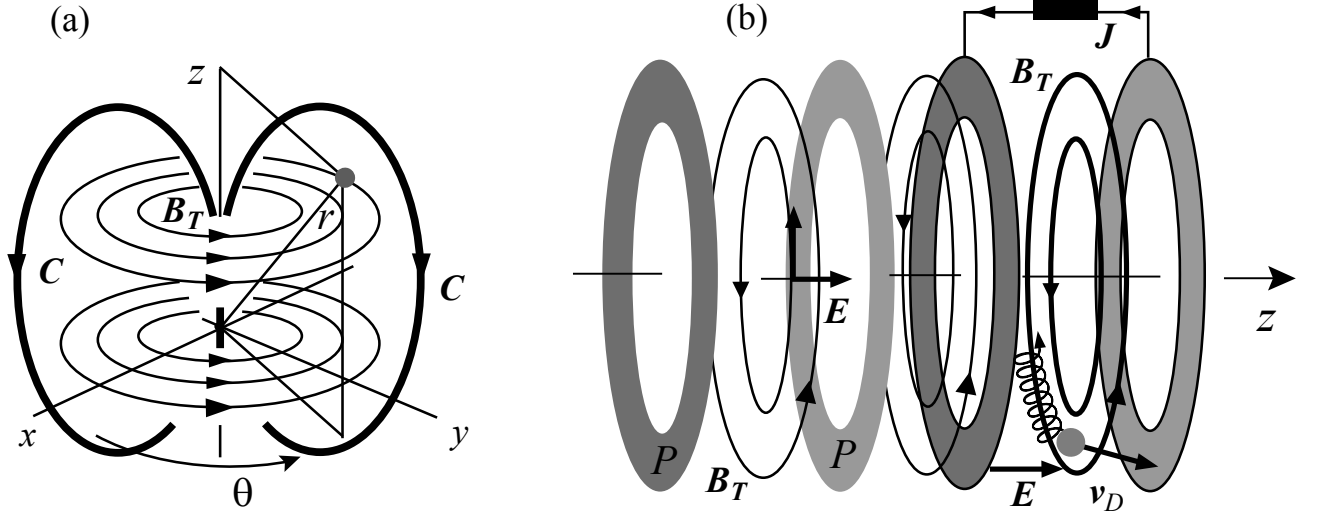


FIG. 5. A toroidal field configuration for DEC; (a) shows the positioning of the coils C used to generate the magnetic field and (b) shows the current-collecting electrode plates P that generate the electric field.

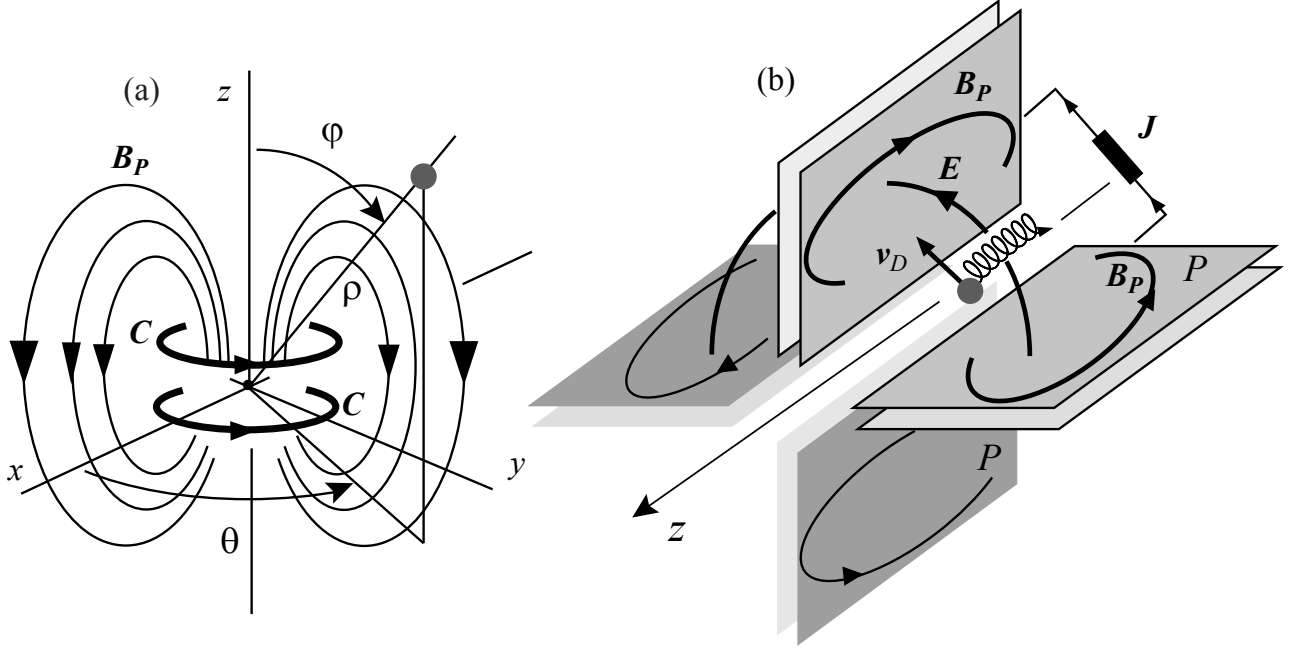


FIG. 6. A poloidal field configuration for DEC; again, (a) shows the positioning of the magnetic field coils C and (b) shows the electrode plates P .

plasma and the electric field is controlled by the sign of the dot product between the drift velocity and the electric field. The condition for plasma cooling and DC power generation is

$$\mathbf{E} \cdot \mathbf{B} \times \nabla B < 0. \quad (7)$$

This can be adjusted in axisymmetric magnetic field configurations through the electrode plates' P positions, shapes and polarizations, so plasma cooling and electric power generation can be envisioned and will be studied in the next sections. In the axisymmetric magnetic field configurations depicted on Fig. 5-(a) and Fig. 6-(a) the

charged particle motion is the drift motion in an inhomogeneous magnetic field and the electric field is sustained between electrode plates P collecting the drift current \mathbf{J} . The azimuthal angle around the Cartesian axis z is denoted by θ ($0 \leq \theta < 2\pi$) and the unit vector \mathbf{e}_θ corresponds to this azimuthal direction. Any axisymmetric magnetic field \mathbf{B} can be represented as the sum of a poloidal plus a toroidal field: $\mathbf{B} = B_T \mathbf{e}_\theta + \nabla \times (A_P \mathbf{e}_\theta)$ where the first term on the right hand side is the toroidal component and the second is the poloidal component. Thus we consider two types of structures aimed at extracting the free energy of a hot plasma and converting it in DC electric power: toroidal and poloidal configurations illustrated respectively in Fig. 5 and Fig. 6. For toroidal generators the electric field is axial, and for poloidal generators the electric field is azimuthal.

In Fig. 5-(b) the $z = \text{constant}$ ring-shaped conducting electrodes P are used to collect the drift current \mathbf{J} in the axial direction. In Fig. 6-(b) the $\theta = \text{constant}$ plane electrodes P are used to collect the drift current \mathbf{J} in the azimuthal direction. With these orientations of the electric and magnetic fields, the adiabatic magnetic drift velocity of the hot charged particles can be directed against the electric field's force to extract thermal energy and cool down the plasma. In both cases this drift current \mathbf{J} provides DC power $\mathbf{J} \cdot \mathbf{E}$ to the external load.

A complete analysis must also take into account the electric $\mathbf{E} \times \mathbf{B}/B^2$ drift. We will see that the impact of this drift is to facilitate energy conversion at low values of E and inhibit it at larger values.

An axisymmetric vacuum magnetic field, $\nabla \times \mathbf{B} = \mathbf{0}$, $\nabla \cdot \mathbf{B} = 0$, $\partial \mathbf{B}/\partial \theta = \mathbf{0}$, either poloidal or toroidal, is locally represented on the Frenet-Serret basis associated with the magnetic field line as $\mathbf{B} = B\mathbf{b}$. The gradient ∇B includes two terms

$$\nabla B = \frac{\partial B}{\partial s} \mathbf{b} + \frac{B}{R} \mathbf{n} \quad (8)$$

where R is the curvature radius of the field line, s is the curvilinear abscissa along the field line and $(\mathbf{b} = \mathbf{B}/B, \mathbf{n} = \partial \mathbf{b}/\partial s)$ are the tangent and normal unit vectors to the field line: the Frenet-Serret moving frame without torsion. The \mathbf{b} component in (8) generates the diamagnetic force along the field lines and the \mathbf{n} component the drift velocity.

In Section III, toroidal magnetic fields will be conveniently described with a cylindrical set of coordinates $[r, \theta, z]$ rather than with the Cartesian one $[x, y, z]$ ($x = r \cos \theta$, $y = r \sin \theta$). The toroidal magnetic field, displayed in Fig. 5-(b), is assumed to be without ripple despite the finite number of coils C

$$\mathbf{B} = B \mathbf{e}_\theta = B_0 \frac{r_0}{r} \mathbf{e}_\theta, \quad (9)$$

$$\mathbf{E} = -\nabla \phi = -E \mathbf{e}_z, \quad (10)$$

where r_0 , E , and B_0 are positive constants. Here we have used Ampère's theorem, $Br = B_0 r_0$ and introduced the

electric potential ϕ . The gradient of the magnetic field strength is directed along the radial direction

$$\nabla B = -\frac{B}{r} \mathbf{e}_r. \quad (11)$$

For a purely toroidal field $\mathbf{n} = -\mathbf{e}_r$, $\partial B/\partial s = 0$ and $R = r$. The poloidal magnetic field configuration illustrated in Fig. 6 and analyzed in Section IV is usually described with spherical coordinates $[\rho, \varphi, \theta]$ rather than cylindrical coordinates $[r, \theta, z]$ ($r = \rho \sin \varphi$, $z = \rho \cos \varphi$). The azimuthal electric field depicted in Fig. 6-(b) can be approximated by

$$\mathbf{E} = -E \mathbf{e}_\theta = -\nabla \phi. \quad (12)$$

The full expression for the field from the electrodes in the figure would include some additional terms, but the simple form given in Eq. (12) is sufficient to show the essential behavior of the energy transfer mechanism. For the poloidal case, we will assume (i) that the source of the thermal plasma is restricted to the region near the equatorial plane $\varphi \sim \pi/2$ in between each pair of plates and (ii) that the field geometry and the conducting electrode plates P are designed such that the capture of the positive and negative charges, above and below this equatorial plane, takes place at a small angle φ . It is convenient to consider the Frenet-Serret representation Eq. (8) in which the radius of curvature of the field lines is denoted by R and the gradient scale length L along the field line is defined as $B/L = \partial B/\partial s$. Along a given field line both the radius R and the length L are functions of s and we will describe the gradient of the magnetic field in the drift region, above and below the equatorial plane, along and across the field lines between the electrodes, with the model

$$\nabla B = \frac{B}{L} \mathbf{b} + \frac{B}{R} \mathbf{n} \quad (13)$$

where rather than the exact functions $L(s)$ and $R(s)$ we consider the average over s of $L(s)$ and $R(s)$ in the region explored by the charged particles in between the equatorial plane and the ultimate capture by the electrodes P at a small angle φ . This approximation makes it simpler to show the dependence of the conversion process on R and L in cases where both are important.

III. ADIABATIC THERMAL ENERGY CONVERSION IN TOROIDAL FIELD

Consider a cylindrical set of coordinates $[R, \theta, z]$ associated with the cylindrical basis $[\mathbf{e}_r, \mathbf{e}_\theta, \mathbf{e}_z]$. The position of a particle with charge q and mass m is given by $R\mathbf{e}_r(\theta) + z\mathbf{e}_z$. The field geometry between two electrodes is illustrated in Fig. 7. We will calculate the thermal energy extraction resulting from the drift-driven electric cooling. The \mathbf{E} cross \mathbf{B} configuration Fig. 7 is described by Eqs. (9,10) where we take $r = R$.

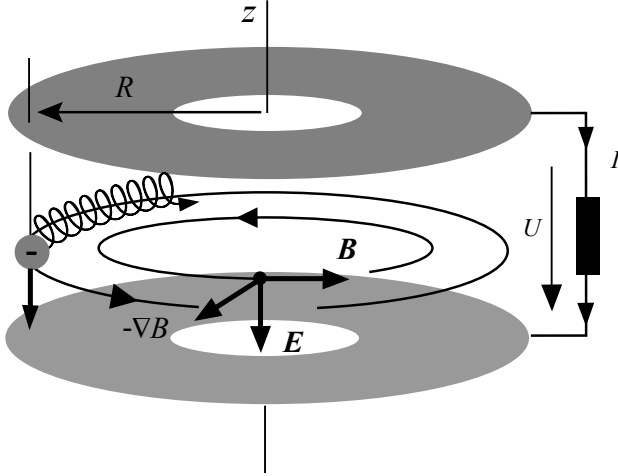


FIG. 7. Schematic of the fields associated with a toroidal field, including the magnetic field-strength gradient and the positions of the current-collecting electrodes.

The gradient of the azimuthal magnetic field strength is radial and is described by Eq. (11)

$$\nabla B = -B_0 \frac{R_0}{R^2} \mathbf{e}_r = -\frac{B}{R} \mathbf{e}_r. \quad (14)$$

The motion of a charged particle in such a toroidal field configuration is a combination of a translation $v_{||}$ along the magnetic field lines, cyclotron rotation v_{\perp} around the field lines and drift \mathbf{v}_D across the magnetic field lines. The total velocity \mathbf{v} is thus given by

$$\mathbf{v} = v_{||} \frac{\mathbf{B}}{B} + \mathbf{v}_D + v_{\perp} \cos(\omega_c t) \mathbf{e}_r + v_{\perp} \sin(\omega_c t) \mathbf{e}_z \quad (15)$$

where $\omega_c = qB/m$ is the cyclotron frequency. The drift velocity \mathbf{v}_D is a combination of the magnetic and electric drifts

$$\mathbf{v}_D = \frac{2\varepsilon_{||} + \varepsilon_{\perp}}{qB^3} \mathbf{B} \times \nabla B + \frac{\mathbf{E} \times \mathbf{B}}{B^2} \quad (16)$$

where we have introduced $\varepsilon_{||} = mv_{||}^2/2$, the kinetic energy along the field lines, and $\varepsilon_{\perp} = mv_{\perp}^2/2$ the cyclotron kinetic energy around the field lines. The axial and radial drift equations are given by

$$\frac{dz}{dt} = \frac{2\varepsilon_{||} + \varepsilon_{\perp}}{qB^3} \mathbf{B} \times \nabla B \cdot \mathbf{e}_z \quad (17)$$

$$\frac{dR}{dt} = \frac{\mathbf{E} \times \mathbf{B}}{B^2} \cdot \mathbf{e}_r \quad (18)$$

The power transfer between the thermal energy and the electric energy is given by the dot product

$$q\mathbf{E} \cdot \mathbf{v}_D = \frac{2\varepsilon_{||} + \varepsilon_{\perp}}{B^3} \mathbf{B} \times \nabla B \cdot \mathbf{E} = -\frac{2\varepsilon_{||} + \varepsilon_{\perp}}{\tau} \quad (19)$$

where we have introduced the secular time scale $\tau > 0$ defined as

$$\tau \doteq \left| \frac{B^3}{\mathbf{E} \times \mathbf{B} \cdot \nabla B} \right| = \frac{B_0 R_0}{E}. \quad (20)$$

The potential energy $q\phi = qEz$ increases in time at the expense of the thermal energy $\varepsilon_{||} + \varepsilon_{\perp}$ so that the sum of the kinetic plus potential energy ε remains constant. Two invariants can be identified: the magnetic moment μ is an adiabatic invariant and the energy ε is a Noether invariant. The cyclotron and total energies can be written as

$$\varepsilon_{\perp}(R) = \mu B(R), \quad (21)$$

$$\varepsilon(z, R) = \varepsilon_{||} + \varepsilon_{\perp} + q\phi(z). \quad (22)$$

We have used the adiabatic ordering and neglected the small drift kinetic energy. The case of a strong electric field, where we take this drift energy into account, is considered in Section VI. Thus as $d\mu/dt = 0$ and $d\varepsilon/dt = 0$, the adiabatic evolution of the energy is described by

$$\frac{d\varepsilon_{\perp}}{dt} = \left[\left(\mathbf{v}_D + v_{||} \frac{\mathbf{B}}{B} \right) \cdot \nabla \right] \mu B, \quad (23)$$

$$\frac{d\varepsilon_{||}}{dt} = - \left[\left(\mathbf{v}_D + v_{||} \frac{\mathbf{B}}{B} \right) \cdot \nabla \right] (q\phi + \mu B). \quad (24)$$

We consider here the slow evolution averaged over the fast cyclotron motion and we have eliminated ε_{\perp} to set up Eq. (24) as $d\varepsilon/dt = 0$. The secular velocity operator involved in Eqs. (23,24) is given by

$$\left(\mathbf{v}_D + v_{||} \frac{\mathbf{B}}{B} \right) \cdot \nabla = \frac{2\varepsilon_{||} + \varepsilon_{\perp}}{qRB} \frac{\partial}{\partial z} + \frac{E}{B} \frac{\partial}{\partial R}, \quad (25)$$

where we note that the $v_{||}$ term drops out due to axisymmetry. We substitute this secular velocity given in Eq. (25) into Eq. (23,24) to get the thermal energy extraction dynamical equations

$$\frac{d\varepsilon_{||}}{dt} = -2\frac{\varepsilon_{||}}{\tau} \quad (26)$$

$$\frac{d\varepsilon_{\perp}}{dt} = -\frac{\varepsilon_{\perp}}{\tau}. \quad (27)$$

We recover the energy balance from Eq. (19).

During the transit of one charged particle toward the electrode, its thermal energy decreases at an exponential rate with respect to time. This behavior provides an efficient way to directly extract the thermal energy. The physics behind this exponential extraction of the thermal energy

$$\varepsilon_{||} + \varepsilon_{\perp} = \varepsilon_{||0} \exp\left(-\frac{2t}{\tau}\right) + \varepsilon_{\perp 0} \exp\left(-\frac{t}{\tau}\right) \quad (28)$$

can be described as follows.

The electric drift E/B is radial and pushes particles toward the lower- B region where $\varepsilon_{\perp} = \mu B$ is converted

into ε_{\parallel} in order to ensure the adiabatic invariance of μ . At the very same time the magnetic drift is axial along z and pushes particles toward high potential $q\phi$ regions where $\varepsilon_{\parallel} + \varepsilon_{\perp}$ decreases in order to ensure the invariance of $\varepsilon = \varepsilon_{\parallel} + \varepsilon_{\perp} + q\phi$. This thermal energy extraction is illustrated in Figure 8.

The drift equations given by Eqs. (17) and (18) can be integrated to give

$$z = z_0 + \frac{\varepsilon_{\parallel 0}}{qE} \left[1 - \exp\left(-\frac{2t}{\tau}\right) \right] + \frac{\varepsilon_{\perp 0}}{qE} \left[1 - \exp\left(-\frac{t}{\tau}\right) \right] \quad (29)$$

and

$$R = R_0 \exp\left(\frac{t}{\tau}\right). \quad (30)$$

These two expressions determine the dimensions of a device needed to access a given extraction efficiency. These relations describe an expansion of the hot plasma and they set limitations on the full thermal energy extraction as the device must display a finite size and footprint. These geometrical limitations will be analyzed in Section V.

IV. ADIABATIC THERMAL ENERGY CONVERSION IN POLOIDAL FIELDS

Before addressing the geometrical and dynamical limitations of the conversion efficiency of the process described by Eq. (28), we explore in this section the main difference between (i) plasma cooling in a toroidal field and (ii) plasma cooling in a poloidal field. Using the model poloidal field described by Eqs. (12,13), the set of relations Eqs. (26,27) describing adiabatic slowing down becomes

$$\frac{d\varepsilon_{\parallel}}{dt} = -2\frac{\varepsilon_{\parallel}}{\tau} - v_{\parallel} \frac{\varepsilon_{\perp}}{L}, \quad (31)$$

$$\frac{d\varepsilon_{\perp}}{dt} = -\frac{\varepsilon_{\perp}}{\tau} + v_{\parallel} \frac{\varepsilon_{\perp}}{L}. \quad (32)$$

We recover the general energy balance from Eq. (19), which is in fact independent of the configuration, poloidal, toroidal or mixed, although in general τ may become a function of s . Compared to Eqs. (26,27), there is an additional term due to the diamagnetic mirror force redistributing the energy between the parallel and cyclotron degree of freedom to ensure μ adiabatic invariance. It is to be noted that, as opposed to the previous toroidal case where the energy relations Eqs. (26,27) are exact in a perfect toroidal field, the poloidal case here is only analyzed on the basis of the approximate model poloidal field Eq. (13). The aim of this section is to identify the impact of a gradient along the field lines.

The additional L term is treated as a small perturbation so that the zero order solutions are just the solutions

of Eqs. (26,27) which fulfills the conservation relation

$$\varepsilon_{\perp}/\sqrt{\varepsilon_{\parallel}} = \varepsilon_{\perp 0}/\sqrt{\varepsilon_{\parallel 0}}. \quad (33)$$

We introduce the characteristic time

$$\tau_0 = \frac{L}{\varepsilon_{\perp 0}} \sqrt{2m\varepsilon_{\parallel 0}}$$

and assume $\tau < \tau_0$. Within the framework of this perturbative expansion the cooling of the parallel energy Eq. (31) becomes

$$\frac{d\varepsilon_{\parallel}}{dt} = -2\frac{\varepsilon_{\parallel}}{\tau} \pm 2\frac{\varepsilon_{\parallel}}{\tau_0}. \quad (34)$$

The analysis of the cooling/conversion process takes place in the $(\varepsilon_{\parallel}, \varepsilon_{\perp})$ energy space. In the toroidal case the *cooling trajectories* in energy space, Eqs. (26,27), are all restricted to parabolic curves in this space

$$\frac{d\varepsilon_{\parallel}}{\varepsilon_{\parallel}} = 2\frac{d\varepsilon_{\perp}}{\varepsilon_{\perp}}. \quad (35)$$

The interesting new phenomenon associated with the occurrence of a gradient of the field strength along the field line (L) is the possibility to shape different cooling trajectories according to

$$\frac{d\varepsilon_{\parallel}}{\varepsilon_{\parallel} (1/\tau \mp 1/\tau_0)} = 2\frac{d\varepsilon_{\perp}}{\varepsilon_{\perp} (1/\tau \pm 2\varepsilon_{\perp}\varepsilon_{\parallel 0}/\varepsilon_{\perp 0}^2\tau_0)}. \quad (36)$$

This new freedom opens the way to an optimization of the final stage of the free energy extraction. The necessity of such an optimization is clearly displayed by the analysis of the evolution of the anisotropy of the particle energy distribution function. Consider a particle with initial parallel, perpendicular, and total energies $\varepsilon_{\parallel 0}$, $\varepsilon_{\perp 0}$, and ε_0 , respectively. Define the initial pitch angle ϑ by

$$\varepsilon_{\parallel 0} = \varepsilon_0 \cos^2 \vartheta, \quad (37)$$

$$\varepsilon_{\perp 0} = \varepsilon_0 \sin^2 \vartheta. \quad (38)$$

This gives $\varepsilon_{\parallel 0} + \varepsilon_{\perp 0} = \varepsilon_0$ by construction. Equipartition of energy between the three directions of motion corresponds to $\vartheta_{\text{EP}} = \arccos(\sqrt{1/3})$. For the previous toroidal case we have found

$$\frac{\varepsilon_{\perp}}{\varepsilon_{\parallel}} = \tan^2 \vartheta \exp\left(\frac{t}{\tau}\right) \quad (39)$$

This increase of the cyclotron energy at the expense of the parallel energy can be controlled if we modulate the purely toroidal field and introduce a new structural freedom with $L(s)$ continuously redistributing the cyclotron energy into the parallel one during the slowing down process. This study of the optimization of the magnetic and electric fields configuration is left for a future work as it must be addressed after a careful assessment of the limitations of the purely toroidal configuration. The next sections (V and VI) are devoted to the analysis of these limitations which are of dynamical and geometrical nature.

V. EFFICIENCY: GEOMETRICAL LIMITATIONS

We can define the efficiency of free energy extraction as the fraction $\eta \leq 1$ of extracted initial thermal energy

$$\eta = 1 - \frac{\varepsilon_{\parallel}(t) + \varepsilon_{\perp}(t)}{\varepsilon_0} \quad (40)$$

$$= 1 - \cos^2 \vartheta \exp\left(-\frac{2t}{\tau}\right) - \sin^2 \vartheta \exp\left(-\frac{t}{\tau}\right). \quad (41)$$

This relation clearly displays the advantage of the possibility to control, independently of the energy dynamics, the pitch angle dynamics ϑ . Such a possibility is offered by a gradient of the field strength along the field line (L) analyzed in Section IV. One major limit on the achievable efficiency η is the time available before a particle strikes a boundary of the device. Following Figure 8, let h be the width of the gap between the two electrodes and ℓ be the radial extent of the circular electrodes.

The transit from the inner edge $R = R_0$ to the outer edge $R = R_0 + \ell$ takes time t_r given by

$$\frac{t_r}{\tau} = \log\left(1 + \frac{\ell}{R_0}\right). \quad (42)$$

A particle could also strike the axial boundary first. The time to transit from $z = z_0$ to $z = z_0 + h$ is

$$\frac{t_z}{\tau} = \log \frac{\sin^2 \vartheta + \sqrt{\sin^4 \vartheta + 4 \cos^2 \vartheta (1 - qEh/\varepsilon_0)}}{2(1 - qEh/\varepsilon_0)} \quad (43)$$

where Eh is the full voltage drop between the electrodes and qEh/ε_0 the ratio of that potential energy to the initial kinetic energy of the particle. Note that the square root is real when $\varepsilon_0 > qEh$. Then this first limit is determined by the efficiency η that can be achieved in the lesser of t_r and t_z (or, in the case where $t_z \notin \mathbb{R}$, it is determined by t_r alone).

This can also be understood as a constraint on the system size required to achieve a particular efficiency η . Consider, for example, the case in which the radial size ℓ is limiting (rather than the axial size h). If $\vartheta = \vartheta_{\text{EP}}$, ℓ and η are related by

$$\frac{\ell}{R_0} = \left(\sqrt{4 - 3\eta} - 1\right)^{-1} - 1. \quad (44)$$

Near-perfect efficiencies would require $\ell \gg R_0$. The axial gap h must also be large enough in order to ensure a significant conversion efficiency η , taking $h = z - z_0$ in Eq. (29) and a thermal distribution with equipartition gives the relation

$$\frac{qEh}{k_B T} = 3/2 - \left(\sqrt{4 - 3\eta} - 1\right)^2 / 2 - \left(\sqrt{4 - 3\eta} - 1\right) \quad (45)$$

Apart from the geometric scaling, the other main constraint on this DEC scheme has to do with the validity of the first order adiabatic drift theory which is analyzed in the next section.

VI. EFFICIENCY: DYNAMICAL LIMITATIONS

To identify the dynamical limit we consider the next order drift within the framework of adiabatic theory: the second-order inertial drift \mathbf{v}_{DI} , which can be written as follows:

$$\mathbf{v}_{DI} = \frac{\mathbf{B}}{qB^2} \times m \frac{d}{dt} \left(\frac{\mathbf{E} \times \mathbf{B}}{B^2} \right) = \frac{m}{qB\tau} \frac{\mathbf{E}}{B}. \quad (46)$$

Here τ is the same timescale introduced in Eq. (20). We recognize here the usual polarization drift associated with the time variation τ . We see that this inertial drift is always along $q\mathbf{E}$ in the direction opposite to the magnetic drift and provides a limiting effect to the previous first order conversion process. This second-order drift does not affect the secular radial dynamics given in Eq. (18), but the secular axial dynamics in Eq. (17) becomes

$$\frac{dz}{dt} = (\mathbf{v}_D + \mathbf{v}_{DI}) \cdot \mathbf{e}_z = \frac{2\varepsilon_{\parallel} + \varepsilon_{\perp}}{qE\tau} - \frac{mE}{qB^2\tau}. \quad (47)$$

For any given particle, the transfer of energy from kinetic energy to the electric field will reverse when $dz/dt = 0$, at which point ($z - z_0 = h^*$, $R = R_0 + l^*$) the device will no longer operate as a DEC generator but as an accelerator for that particle. This reversal of the energy transfer is illustrated in Fig. 9.

The power transfer between the thermal energy and the electric energy is given by the dot product $q\mathbf{E} \cdot (\mathbf{v}_D + \mathbf{v}_{DI})$:

$$qE \frac{dz}{dt} = \frac{2\varepsilon_{\parallel} + \varepsilon_{\perp}}{\tau} - \frac{mE^2/B^2}{\tau}. \quad (48)$$

We define the drift energy as

$$\varepsilon_{E/B} = \frac{m}{2} \frac{E^2}{B^2}. \quad (49)$$

To study the limitation associated with this reversal of the energy transfer, we now consider the case in which the $\mathbf{E} \times \mathbf{B}$ drift may contain a significant fraction of the kinetic energy, in which case the leading-order expression for energy becomes

$$\varepsilon(z, R) = \varepsilon_{\parallel} + \varepsilon_{\perp} + \varepsilon_{E/B} + q\phi \quad (50)$$

rather than Eq. (22). The leading-order expression for energy conservation ought to be

$$\frac{d}{dt} (\varepsilon_{\parallel} + \mu B + q\phi + \varepsilon_{E/B}) = 0 \quad (51)$$

Thus Eqs. (23) and (24) are replaced by

$$\frac{d\varepsilon_{\parallel}}{dt} = - \left[\left(\mathbf{v}_D + \mathbf{v}_{DI} + v_{\parallel} \frac{\mathbf{B}}{B} \right) \cdot \nabla \right] \left(q\phi + \mu B + \frac{m}{2} \frac{E^2}{B^2} \right) \quad (52)$$

and

$$\frac{d\varepsilon_{\perp}}{dt} = \left[\left(\mathbf{v}_D + \mathbf{v}_{DI} + v_{\parallel} \frac{\mathbf{B}}{B} \right) \cdot \nabla \right] \mu B \quad (53)$$

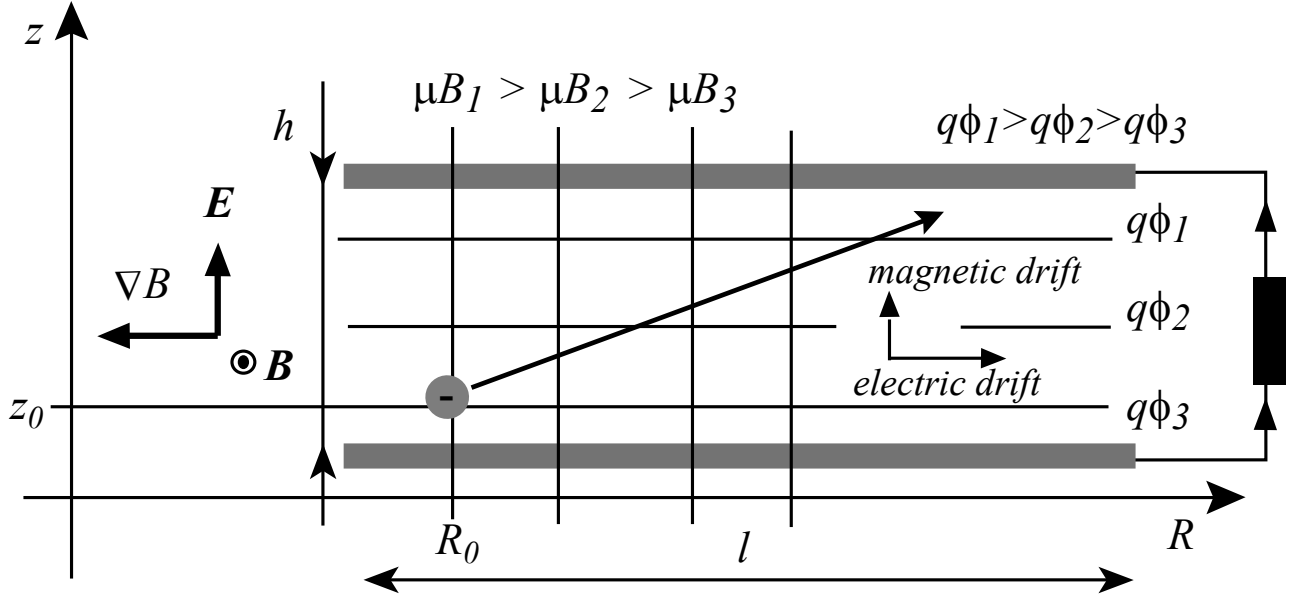


FIG. 8. The trajectory of a particle as it moves between the electrodes includes both magnetic and electric drift motion.

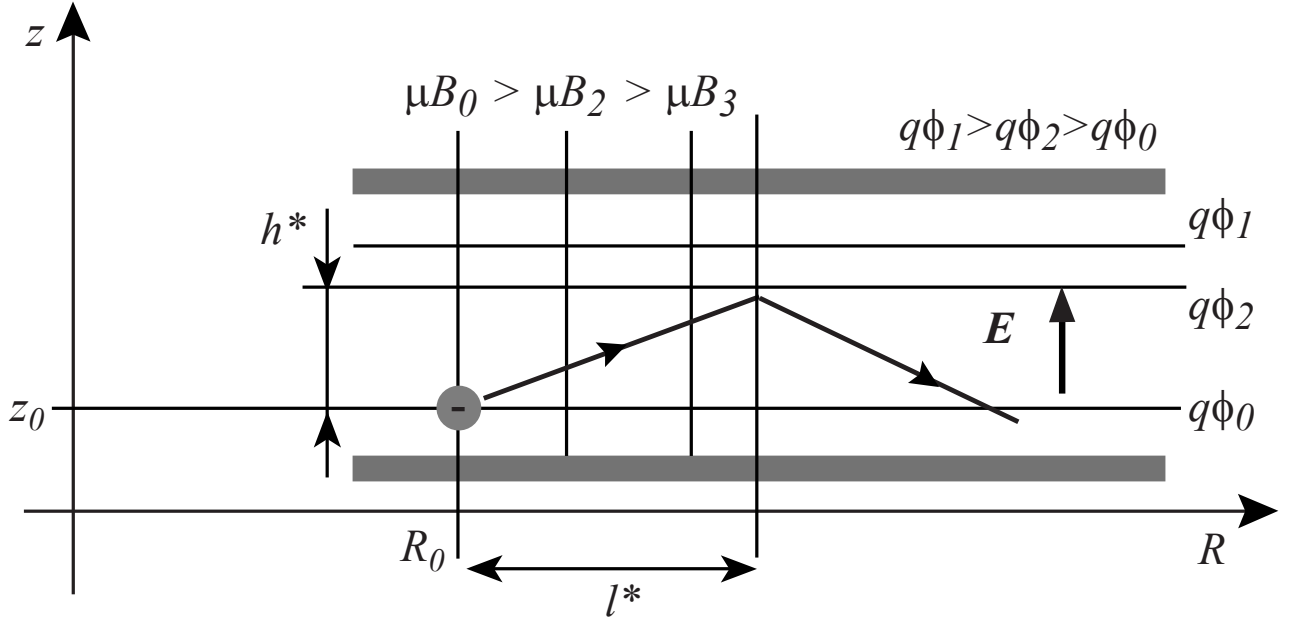


FIG. 9. A dynamical limitation of this DEC scheme: if a particle is allowed to move too far without striking an electrode, the energy transfer will reverse and the particle will start to take energy from the fields rather than transferring energy to the fields.

completed by the inertial/polarization drift effect

$$\frac{d\varepsilon_{E/B}}{dt} = \left[\left(\mathbf{v}_D + \mathbf{v}_{DI} + v_{\parallel} \frac{\mathbf{B}}{B} \right) \cdot \nabla \right] \left(\frac{m}{2} \frac{E^2}{B^2} \right) \quad (54)$$

where

$$\left(\mathbf{v}_D + \mathbf{v}_{DI} + v_{\parallel} \frac{\mathbf{B}}{B} \right) \cdot \nabla = \left(\frac{2\varepsilon_{\parallel} + \varepsilon_{\perp}}{qE\tau} - \frac{mE}{qB^2\tau} \right) \frac{\partial}{\partial z} + \frac{E}{B} \frac{\partial}{\partial R}, \quad (55)$$

rather than Eq. (25).

The evolution of the thermal parallel and perpendicular cyclotron energies fulfill

$$\frac{d\varepsilon_{\parallel}}{dt} = -\frac{2\varepsilon_{\parallel}}{\tau}, \quad (56)$$

$$\frac{d\varepsilon_{\perp}}{dt} = -\frac{\varepsilon_{\perp}}{\tau}. \quad (57)$$

Note that this ε_{\perp} is the part of the kinetic energy in the Larmor gyration, not the total kinetic energy in the perpendicular direction (which also includes drift motion contribution $\varepsilon_{E/B}$). The evolution of $\varepsilon_{E/B}$ Eq. (54) is given by

$$\frac{d\varepsilon_{E/B}}{dt} = \frac{2\varepsilon_{E/B}}{\tau}. \quad (58)$$

It can be checked that Eqs. (51,48) are consistent with Eqs. (56,57,58) as $Ez = \phi$. These equations (56,57,58) can be integrated directly. The three components of the kinetic energy evolves respectively according to

$$\varepsilon_{\parallel} = \varepsilon_{\parallel 0} \exp\left(-\frac{2t}{\tau}\right), \quad (59)$$

$$\varepsilon_{\perp} = \varepsilon_{\perp 0} \exp\left(-\frac{t}{\tau}\right), \quad (60)$$

$$\varepsilon_{E/B} = \frac{\varepsilon_0}{2C} \exp\left(\frac{2t}{\tau}\right), \quad (61)$$

where we have defined the constant

$$C \doteq \frac{\varepsilon_0 B_0^2}{mE^2}. \quad (62)$$

The transfer of kinetic to potential energy is

$$\begin{aligned} qE(z - z_0) &= \varepsilon_{\parallel 0} \left[1 - \exp\left(-\frac{2t}{\tau}\right) \right] \\ &+ \varepsilon_{\perp 0} \left[1 - \exp\left(-\frac{t}{\tau}\right) \right] \\ &+ \frac{mE^2}{2B_0^2} \left[1 - \exp\left(-\frac{2t}{\tau}\right) \right]. \end{aligned} \quad (63)$$

The key effect captured by the inclusion of \mathbf{v}_{DI} is that the increase in $\mathbf{E} \times \mathbf{B}$ flow energy, as the particle moves outwards, tends to slow and eventually reverse the transfer from kinetic to potential energy.

The time t^* at which this reversal takes place is given by $dz/dt = 0$ in (48)

$$2\varepsilon_{\parallel}(t^*) + \varepsilon_{\perp}(t^*) = \frac{mE^2}{B^2} = \frac{mE^2}{B_0^2} \exp\left(\frac{2t^*}{\tau}\right) \quad (64)$$

so that we have to solve

$$2C \cos^2 \vartheta + C \sin^2 \vartheta \exp\left(\frac{t^*}{\tau}\right) = \exp\left(\frac{4t^*}{\tau}\right). \quad (65)$$

in order to find t^* . Numerical solutions of Eq. (65) for the cases of $\vartheta = 0$, $\vartheta = \vartheta_{EP}$, and $\vartheta = \pi/2$ are shown in Fig. 10.

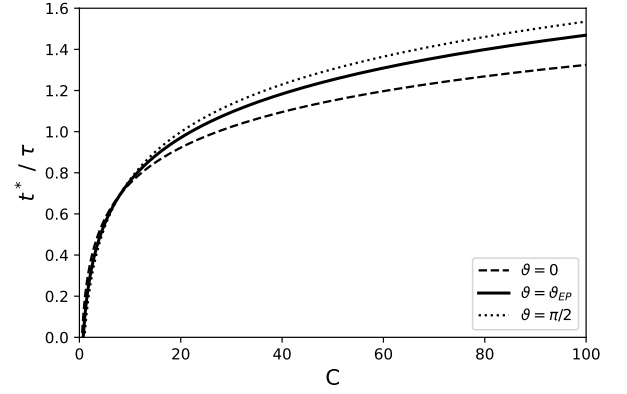


FIG. 10. The critical time t^* after which the energy transfer reverses, as a function of the dimensionless parameter C . The curves shown here take $\vartheta = 0$, $\vartheta = \vartheta_{EP}$, and $\vartheta = \pi/2$, respectively.

The logarithmic behavior of this numerical solution describing the initial equipartition case reflects the behavior of the particular solutions associated respectively with $\vartheta = 0$ and $\vartheta = \pi/2$:

$$\left. \frac{t^*}{\tau} \right|_{\vartheta=0} = \log(2C)/4, \quad (66)$$

$$\left. \frac{t^*}{\tau} \right|_{\vartheta=\pi/2} = \log(C)/3. \quad (67)$$

The maximum free energy extraction efficiency in a large device, free of the geometrical limitations analyzed in the previous section, is

$$\eta^*(E, B_0, \varepsilon_0, \vartheta) = 1 - \cos^2 \vartheta \exp\left(-\frac{2t^*}{\tau}\right) - \sin^2 \vartheta \exp\left(-\frac{t^*}{\tau}\right) \quad (68)$$

Numerical solutions for this maximum efficiency $\eta^*(C)$ for a large device are shown on Fig. 11 for the cases of $\vartheta = 0$, $\vartheta = \vartheta_{EP}$, and $\vartheta = \pi/2$.

The algebraic behavior of the type $1 - \alpha C^{-\beta}$ of this numerical solution describing the initial equipartition case reflects the behavior of the particular solutions associated respectively with $\vartheta = 0$ and $\vartheta = \pi/2$:

$$\eta^*(\vartheta = 0) = 1 - C^{-\frac{1}{2}}/\sqrt{2} \quad (69)$$

$$\eta^*(\vartheta = \pi/2) = 1 - C^{-\frac{1}{3}} \quad (70)$$

The efficiency of a real device will depend on the birth distribution of charged particles both in $(\varepsilon_0, \vartheta)$ space and in spatial position (z_0, R_0) . For any birth distribution, it is clear that this effect will reduce the realizable efficiency. This can be understood as a limitation on the current-voltage (I - U) curve describing the operation of an adiabatic DEC generator. The total voltage drop of the configuration can be increased either by increasing E or by increasing h . For any given starting condition

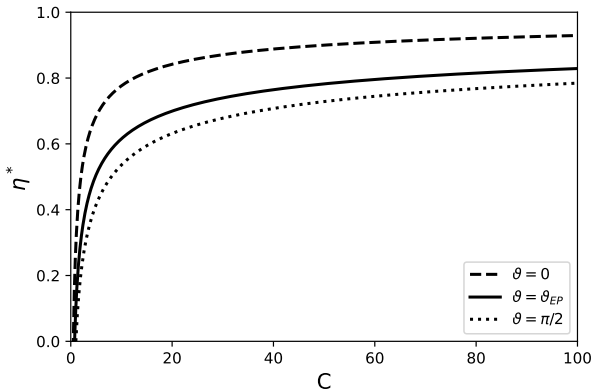


FIG. 11. The maximum free energy extraction efficiency as a function of the dimensionless parameter C for selected values of ϑ . This maximum takes into account dynamical but not geometrical constraints (that is, it assumes an optimally large device).

$(\varepsilon_0, \vartheta)$, if either E or h is increased beyond some threshold, the particle will not reach the collection plate before its trajectory reverses. Note, however, that although increasing either E or h will increase the total voltage drop, and either will eventually cause electrons to turn before they reach the negative electrode, these two parameters influence the dynamics in different ways. E and h both change the total energy that must be extracted before a particle can traverse a given axial distance, but changing E also modifies the feedback from the inertial drift.

If all electrons reach the negatively charged electrode, then the total device current I is set by the rate of ionization events or the rate of charged particles incoming flow, and I is independent of U . However, as U increases, there is a threshold (which will depend on the birth distribution of the charged particles and of the size, field strength and shape of the configuration) where I will quickly drop off as a result of electrons turning before they can reach the negative electrode. Qualitatively, this will produce an I - U characteristic like the one pictured in Figure 12, though one should keep in mind that the details of this curve will depend on not only the details of the birth distribution but also on what is held fixed when the voltage is increased. For any particular case, this curve makes it possible to determine the highest-power operating point; one can draw the set of isopower hyperbolae $IU = \text{constant}$ and select the one that is tangent to the convex I - U generator characteristic.

In the most idealized case, in which the birth distribution is monoenergetic and all particles are born at the same spot and with the same ϑ , the I - U curve is a step function with constant $I = I_0$ for all $U < V_0$, then $I = 0$ for all $U \geq V_0$ (with V_0 corresponding to the threshold at which the particles turn before reaching the boundary $dz/dt = 0$). In this case, the highest-power operating point corresponds to the corner of the

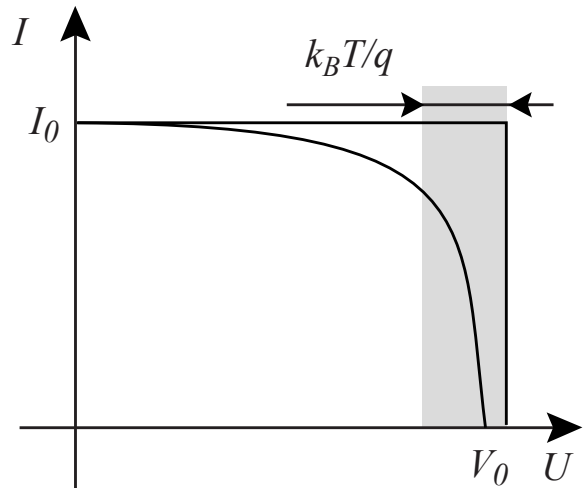


FIG. 12. The current-voltage characteristic for a DEC generator of this type is initially flat, with little dependence of the current on the voltage. At higher voltages, the output current drops as a function of voltage.

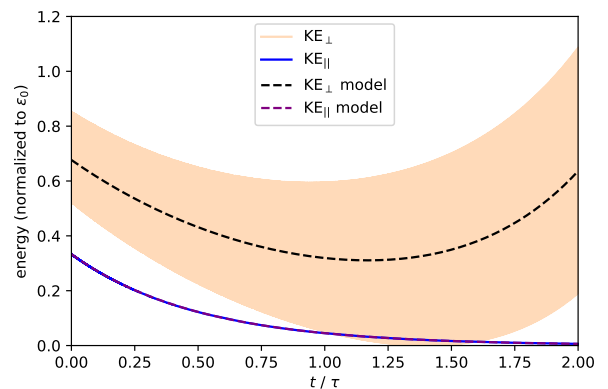


FIG. 13. Numerical validation of the analytic model using a single-particle simulation. This case had $C = 50$, from which we would expect a turning point at $t \approx 1.253\tau$. The region colored in by the KE_\perp curve is the result of fast oscillations due to the gyrophase-dependent orientations of the Larmor motion and the drift motion.

I - U curve, with $P = I_0 V_0$. For the case of a radiation driven plasma generation, this power would be a linear function of the absorbed radiation (since this would determine the total number of ionization events). From Eq. (47), $dz/dt = 0$ implies that $mE^2/B^2 = \mathcal{O}(k_B T)$, so that $V_0 = Eh = \mathcal{O}(B_0 v_{th} h)$, where v_{th} is the thermal velocity.

The previous analytic calculations can be validated numerically using single-particle simulations. Figure 13 shows one such example.

The simulation showed in the figure used a single-particle Boris pusher and had $C = 50$ and $\vartheta = \vartheta_{EP}$.

Note that for these parameters, Eq. (65) can be solved numerically to yield $t^* \approx 1.253\tau$. This is consistent with the turning point seen in the simulation. The fluctuations in the numerically observed KE_{\perp} about the model are the result of the gyrations of the particle. Depending on the gyrophase, the Larmor motion can have either positive or negative radial components.

The energy in the perpendicular motion can only be decomposed into gyration energy and drift-motion energy on average. The kinetic energy used for the model in the figure includes both ε_{\perp} and $mE^2/2B^2$.

These simulations confirm the validity of the previous analytical model and points toward the necessity to consider an additional possibility to convert the cyclotron energy into the parallel energy. We have seen in Section IV that a gradient of the field strength along the field line offers such a possibility and this optimization strategy will be explored in a forthcoming study.

VII. RADIATION FLUX AND PLASMA FLOW HEAT CONVERSION

In this section we briefly describe two types of adiabatic DEC implementation in $^2D/^3T$ tokamak reactors and in aneutronic $^1P/^11B$ reactors.

In a tokamak reactor the hot thermonuclear plasma diffuses from the confining closed field line to the open field lines of the divertor. The last closed flux surface (LCFS) defines the boundary of the confining toroidal configuration. The set of diverted field lines defines open magnetic surfaces illustrated in Fig. 14.

Far from the X point line, the magnetic field in the outer part of the divertor, illustrated in Fig. 14, is toroidal and a dedicated set of upper and lower electrodes can polarize these magnetic surfaces such that they become also equipotential surfaces Ψ_1, Ψ_2, Ψ_3 . In doing so we have realized the geometry of a toroidal generator and we can envision to extract part of the free enthalpy of the divertor plasma flow in such a configuration. This geometry of an advanced divertor requires a far more detailed analysis which is left to a future work.

Let us now consider the case of rotating mirror $^1P/^11B$ reactors. Because of the high temperature, the thermonuclear plasma column is strongly radiating both in the microwave range, as a result of electron cyclotron/synchrotron emission, and in the UV-X range, as a result of electron bremsstrahlung. Keeping the axisymmetric geometry (Fig. 6-(b)) we can design a conversion blanket all around this magnetized radiating plasma column where the escaping intense radiation will ionize a vapor, for example cesium vapor, and heat the associated plasma. The escaping radiation can also be absorbed by metal target plates, for example tungsten plates, and the resulting hot metal plate can act as an hot electron source whose energy is converted by the E cross B poloidal configuration of the conversion blanket.

Various toroidal, poloidal and mixed declinations of

the E cross B configurations can be adapted to both $^2D/^3T$ tokamak reactors and in aneutronic $^1P/^11B$ reactors. The identification of the most relevant designs can not be addressed on the basis of the simple discussion of this section and is left for a future study.

VIII. CONCLUSION

To summarize our results, we suggest a novel technique for converting power from plasma and radiation to electricity. A technology that could efficiently capture and convert power from plasma and radiation to electricity could be useful in a wide variety of applications. For example, magnetic confinement fusion typically involves heating plasmas to temperatures at which radiative losses can be significant. The ability to recapture this energy could be most critically important for reactors burning aneutronic fuels, which often require higher temperatures with correspondingly higher radiative losses. For instance, bremsstrahlung and synchrotron losses are a major hurdle for economical p- ^{11}B fusion [23–26]. In very hot fusion plasmas, measures have been proposed to suppress this radiation primarily through plasma absorption and redirection to kinetic energy, as well as through suppression of the population of high-energy electrons [27–30]. However, the direct energy conversion schemes here could, in principle, act synergistically with these other techniques. The manipulation of the plasma 6D phase space has been recognized as necessary for making economical fusion through high temperature aneutronic fusion approaches in general [31], and the techniques proposed here can be imagined working either separately or in concert with these phase space techniques.

For a hot plasma such that $k_B T \sim \varepsilon_0$, the design of a generator implies the choice of (i) the geometrical characteristics (R_0, l, h), and of (ii) the field strengths (E, B_0). We have found that the various physical and geometrical constraints are in fact functions of the two control parameters $\tau = B_0 R_0 / E$ and $C = \varepsilon_0 B_0^2 / m E^2$. The description of the poloidal-geometry dynamics requires a third control parameter $\tau_0 = L \sqrt{2m\varepsilon_{||0}} / \varepsilon_{\perp 0}$. The poloidal geometry displays an additional advantage over the toroidal one as the cyclotron energy can be continuously converted into parallel energy. Such a possibility is advantageous because E cross B configurations convert the parallel energy to DC electric power at a far faster rate than the cyclotron (perpendicular) energy. The design of an optimal field is clearly the next question to be addressed to identify efficient E cross B conversion schemes for both $^2D/^3T$ tokamak and $^1P/^11B$ advanced reactors.

The idea of poloidal and toroidal DEC rests on the tendency of the ∇B drift to carry particles in different directions depending on the sign of their charge. Its implementation in $^1P/^11B$ advanced reactors relies on radiative ionization and heating. Radiation can deposit significant energy, after ionization, in the resulting ions and electrons.

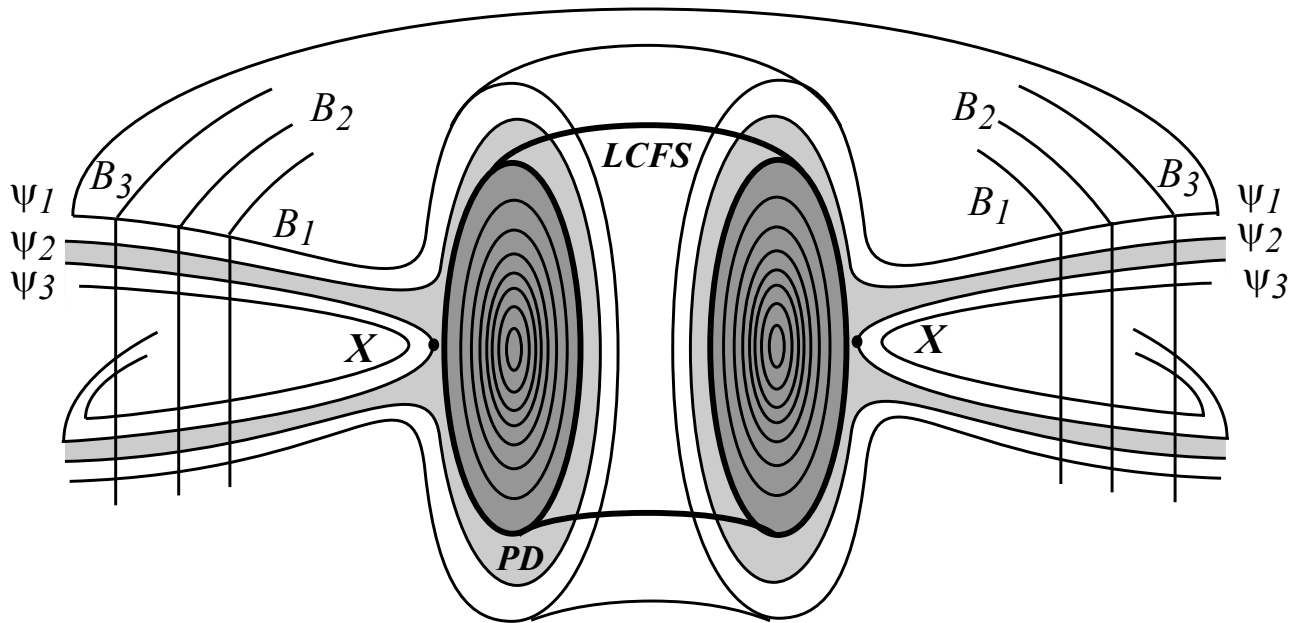


FIG. 14. A schematic of the magnetic flux surfaces in a tokamak, with the last closed flux surface (LCFS) marked.

Note that the transfers of energy considered here – e.g., between kinetic energy and electric fields – are all adiabatic. This can be contrasted with work (such as the alpha-channeling concept [32]) that instead accomplishes this transfer using resonant interactions.

This adiabatic transfer process – like all energy-conversion processes – will not be perfectly efficient. In this paper, we have considered two constraints on the performance of an adiabatic DEC device. The first is a matter of geometry: the charged particles need enough space to give up as much kinetic energy as possible before hitting a boundary of the device. Even in the absence of any other constraints, this is enough to prevent any realistic device from attaining perfect efficiency, since progressively better efficiencies require exponentially increasing device sizes.

We also considered a dynamical constraint, wherein inertial drifts eventually slow (and subsequently reverse) the energy extraction process. The characteristic timescale involved depends on the parameter C . The highest efficiencies require higher values of C .

There are a variety of additional constraints and engineering challenges not considered here. For example, this kind of device relies on the presence of a large enough population of neutral particles to absorb and be ionized by the incoming radiation. However, if that population were too large, collisions between charged and neutral particles would degrade the efficiency of the device.

In addition, a birth distribution of charged particles

that is anything other than a delta function in r , z , ε_0 , and ϑ will make it more difficult to efficiently tune the device parameters. For example, this would mean that different particles' trajectories would turn at different axial and radial positions.

However, these engineering challenges can likely be mitigated by careful control over the device geometry and the composition of the neutral population. The refinement and optimization of these ideas are planned in future work. Moreover, even relatively modest efficiencies could be an exciting development, particularly for applications in which the relevant radiation has wavelengths not amenable to other conversion techniques.

ACKNOWLEDGMENTS

This work was supported by ARPA-E grant no. DE-AR0001554. JMR further acknowledges the hospitality of Princeton University and support from the Andlinger Center for Energy and the Environment through an ACEE fellowship, under which this work was initiated. EJK acknowledges the support of the DOE Fusion Energy Sciences Postdoctoral Research Program, administered by the Oak Ridge Institute for Science and Education (ORISE) and managed by Oak Ridge Associated Universities (ORAU) under DOE contract no. DE-SC0014664.

-
- [1] E. A. Guggenheim, *Thermodynamics* (North Holland Publishing Company, Amsterdam, 1977).
 - [2] H. B. Callen, *Thermodynamics and an Introduction to Thermostatistics* (John Wiley and Sons, New York, 1985).
 - [3] B. Sorensen, *Renewable Energy Conversion Transmission and Storage* (Academic Press, Amsterdam, 2007).
 - [4] R. Decher, *Energy conversion systems, flow physics and engineering* (Oxford University Press, Oxford, 1994).
 - [5] I. I. Novikov, Efficiency of an atomic power generating installation, *Sov. J. At. Energy* **3**, 1269 (1957).
 - [6] P. Chambadal, *Les centrales nucléaires* (Armand Colin, Paris, 1957).
 - [7] F. L. Curzon and B. Ahlborn, Efficiency of a Carnot engine at maximum power output, *Am. J. Phys.* **43**, 22 (1975).
 - [8] J.-M. Rax, *Physique de la conversion d'énergie* (EDP Sciences, Les Ulis, France, 2012).
 - [9] G. W. Sutton, *Direct energy conversion* (McGraw-Hill Book Company, Paris, 1966).
 - [10] R. Decher, *Direct energy conversion fundamentals of electric power production* (Oxford University Press, Oxford, 1997).
 - [11] L. J. Perkins, G. H. Miley, and B. E. Logan, Novel fusion conversion methods, *Nuclear Instruments and Methods in Physics Research* **A271**, 188 (1988).
 - [12] H. Takeno, K. Ichimura, S. Nakamoto, Y. Nakashima, H. Matsuura, J. Miyazawa, T. Goto, Y. Furuyama, and A. Taniike, Recent advancement of research on plasma direct energy, *Plasma and Fusion Research* **14**, 2405013 (2019).
 - [13] H. Momota, Y. Tomita, M. Ishikawa, and Y. Yasaka, A traveling wave direct energy converter for D-3HE fueled fusion reactor, *Fusion Technology* **35:1T**, 60 (1999).
 - [14] K. Yoshikawa, S. Kouda, Y. Yamamoto, and K. Maeda, Development of a two-dimensional particle trajectory code and application to a design of a plasma direct energy converter in the fusion engineering facility based on mirror plasma confinement, *Fusion Technology* **14:2P1**, 264 (1988).
 - [15] V. I. Volosov, Recuperation of charged particle energy in traps with rotating plasma, *Trans. Fusion Sci. Tech.* **47**, 351 (2005).
 - [16] A. V. Timofeev, A scheme for direct conversion of plasma thermal energy into electrical energy, *Fiz. Plazmy* **4**, 351 (1978).
 - [17] S. Dushman, Electron emission from metals as a function of temperature, *Phys. Rev.* **21**, 623 (1923).
 - [18] G. N. Hatsopoulos and E. P. Gyftopoulos, *Thermionic energy conversion* (MIT Press, Cambridge, 1973).
 - [19] F. G. Balsht, G. A. Dyuzhev, A. M. Martsinovskiy, B. Y. Moyzhes, E. B. Sonin, and V. G. Yur'Yev, *Thermionic converters and low-temperature plasma*, Tech. Rep. (Technical Information Center, US-DoE, Washington, 1978).
 - [20] A. V. Nedospasov, The physics of MHD generators, *Sov. Phys. Usp.* **20**, 861 (1977).
 - [21] G. W. Sutton and A. Sherman, *Engineering magnetohydrodynamics* (Dover Publication Inc, New York, 1965).
 - [22] R. J. Rosa, *Magnetohydrodynamic energy conversion* (McGraw-Hill Book Company, New York, 1968).
 - [23] S. V. Putvinski, D. D. Ryutov, and P. N. Yushmanov, Fusion reactivity of pB^{11} plasma revisited, *Nucl. Fusion* **59**, 076018 (2019).
 - [24] E. J. Kolmes, I. E. Ochs, and N. J. Fisch, Wave-supported hybrid fast-thermal $p^{11}B$ fusion, *Phys. Plasmas* **29**, 110701 (2022).
 - [25] I. E. Ochs, E. J. Kolmes, M. E. Mlodik, T. Rubin, and N. J. Fisch, Improving the feasibility of economical proton-boron-11 fusion via alpha channeling with a hybrid fast and thermal proton scheme, *Phys. Rev. E* **106**, 055215 (2022).
 - [26] I. E. Ochs and N. J. Fisch, Lowering the reactor breakeven requirements for proton-boron 11 fusion, *Phys. Plasmas* **31**, 012503 (2024).
 - [27] V. I. Volosov, Aneutronic fusion on the base of asymmetrical centrifugal trap, *Nucl. Fusion* **46**, 820 (2006).
 - [28] M. E. Mlodik, V. R. Munirov, T. Rubin, and N. J. Fisch, Sensitivity of synchrotron radiation to the superthermal electron population in mildly relativistic plasma, *Phys. Plasmas* **30**, 043301 (2023).
 - [29] V. R. Munirov and N. J. Fisch, Suppression of bremsstrahlung losses from relativistic plasma with energy cutoff, *Phys. Rev. E* **107**, 065205 (2023).
 - [30] I. E. Ochs and N. J. Fisch, Electron tail suppression and effective collisionality due to synchrotron emission and absorption in mildly relativistic plasmas, *Phys. Plasmas* **31**, 083303 (2024).
 - [31] H. Qin, Advanced fuel fusion, phase space engineering, and structure-preserving algorithms, *Phys. Plasmas* **31**, 050601 (2024).
 - [32] N. J. Fisch and J.-M. Rax, Interaction of energetic alpha particles with intense lower hybrid waves, *Phys. Rev. Lett.* **69**, 612 (1992).